JOURNAL OF GEOPHYSICAL RESEARCH, VOL. 115, D11112, doi:10.1029/2009JD012611, 2010



# Effects of interbasin water transfer on regional climate: A case study of the Middle Route of the South-to-North Water Transfer Project in China

Feng Chen[1,2,3] and Zhenghui Xie[1,2]

Received 8 June 2009; revised 4 January 2010; accepted 7 January 2010; published 12 June 2010.

[1] In this study, a water transfer mechanism was implemented into the regional climate model, RegCM3, to represent water to be transferred by increasing the precipitation that reached the surface in intake areas. The effects of interbasin water transfer on local and regional climates were then studied based on numerical simulations conducted using the RegCM3 model. The Middle Route of the South-to-North Water Transfer Project (MRSNWTP) in China was chosen as a case study to investigate the climatic responses under three different water transfer schemes with three intensities. Four 10-year simulations were conducted, a control run (MCTL) without water transfer, and three water transfer runs (MWT1, MWT2, and MWT3) related to the three schemes. In the three water transfer runs, spatial and temporal water transfer data were derived from the schemes under the assumption that the quantity of water to be transferred into a county in the intake area in a year for each scheme was distributed evenly into each time step. Increases in top-layer soil moisture and latent heat flux were observed when compared to the control, and these increases were found to occur as a direct result of injecting water into the intake area. The increases in latent heat flux and evaporation were accompanied with decreases in sensible heat flux, mean air temperature, and increases in precipitation in the intake area. These differences were generally small and statistically insignificant, indicating that the water transfer plays a small role in influencing regional climate in our simulations. However, the climatic influence intensity of a water transfer scheme was found to be positively related to the quantity of water to be transferred, and to have strong seasonal variability, with larger effect being observed in spring and autumn than in summer and winter. We also conducted a water transfer run, MWT4, using the same configuration as MWT3 but under the assumption that the quantity of water was distributed evenly into each time step of the first half of the year. Comparison of the two runs shows a stronger seasonal variability in the climatic influence when the water was assigned into the first half of the year than when it was assigned into the entire year. Further analysis revealed that the water transfer could reduce both the seasonal and diurnal temperature ranges at the surface and that the decrease in temperature could diffuse over almost the entire Huabei Plain below 700 hPa, thereby weakening the wind velocity of the easterly breeze. It follows from the analyses of the vertical profiles of the water vapor content and the atmospheric moisture budgets that the water transfer can affect the local and regional climates by changing the local water vapor content and the regional water vapor transports, which in turn influences precipitation.

**Citation:** Chen, F., and Z. Xie (2010), Effects of interbasin water transfer on regional climate: A case study of the Middle Route of the South-to-North Water Transfer Project in China, *J. Geophys. Res.*, *115*, D11112, doi:10.1029/2009JD012611.

## 1. Introduction

[2] To alleviate water resource problems such as water shortages and uneven distribution, more than 345 water transfer projects have been built worldwide (not including projects involving a main canal length of less than 20 km or a water transfer quantity of less than 10 million $m^3$/yr) since the 1950s [*Yang and Liu*, 2003]. *Yang and Liu* [2003] found that the quantity of water transferred reached 597 billion $m^3$/yr, which is approximately 1.4% of the total runoff worldwide.

[1]International Center for Climate and Environmental Sciences, Institute of Atmospheric Physics, Chinese Academy of Sciences, Beijing, China.
[2]Also at State Key Laboratory of Numerical Modeling for Atmospheric Sciences and Geophysical Fluid Dynamics, Institute of Atmospheric Physics, Chinese Academy of Sciences, Beijing, China.
[3]Also at Graduate School of Chinese Academy of Sciences, Beijing, China.


0148-0227/10/2009JD012611

Furthermore, they found that the area irrigated using transferred water reached 55.6 million $hm^2$ in 2002. The South-to-North Water Transfer Project (SNWTP) is one of the most important water transfer projects in the world. The SNWTP consists of an east route, a middle route, and a west route that are designed to deliver water from the south of China to the water-short north to support sustainable social and economic development in northern China [*Yao and Chen*, 1982; *Liu*, 1994; *Liu and Zheng*, 2002]. The Middle Route of the South-to-North Water Transfer Project (MRSNWTP) will transfer water from the Danjiangkou reservoir on the Hanjiang River, which is a large tributary to the middle reaches of the Yangtze River, to Hubei, Henan, and Hebei provinces, and ultimately to Beijing and Tianjin [*Changjiang Water Resources Commission*, 2001a]. This type of large-scale interbasin water transfer will likely change the basins involved by disrupting the old water balance and creating new hydrological cycles. As a result, these human activities will impact the hydrology, climate, ecology, and environment of the region through changes in the soil moisture and water and energy balances between the land surface and the atmosphere [*Wang and Ma*, 1999; *Wang et al.*, 2006; *Shan et al.*, 2007].

[3] When water to be transferred is used for irrigation, it increases the latent heat flux and decreases the sensible heat flux at the surface, thereby reducing the surface air temperatures [*Li et al.*, 1980; *Yeh et al.*, 1984; *Pielke et al.*, 2002; *Adegoke et al.*, 2003; *Boucher et al.*, 2004; *Lobell et al.*, 2006; *Bonfils and Lobell*, 2007; *Kueppers et al.*, 2007]. Large-scale irrigation affects the distribution of evaporation as well as the distributions of temperature and precipitation, and anomalies of soil moisture created by irrigation can persist for at least several months [*Yeh et al.*, 1984]. To investigate the potential effects of water transfer along the east route of the SNWTP, *Li et al.* [1980] accounted for the water to be transferred as irrigation water in an energy balance equation under the assumption that the project leads to 100 mm/month more irrigation water in the dry season. *Zhao* [2002] investigated the local climate variation induced by the increase in soil moisture from the SNWTP using a one-dimensional energy equilibrium model in an air column. *Chen et al.* [2005] implemented the water to be transferred as additional precipitation using surface water and energy balance models to explore the potential climatic influences of the SNWTP in northern China. Those studies of the SNWTP used one-dimensional surface or energy equilibrium models in which the effects of large-scale water transfer on regional atmospheric circulation and climate have not been well quantified, particularly at regional scales. Accordingly, it is necessary to improve the understanding of how interbasin water transfer influences regional climate for guiding policies aimed at mitigating or adapting to climate change.

[4] Several studies have been conducted to investigate the effects of irrigation on climate using climate models, but they have treated irrigation water in different ways. For example, *Yeh et al.* [1984] simulated the effect of large-scale irrigation on short-term changes in hydrology and climate using the simple general circulation model [*Manabe and Stouffer*, 1980; *Wetherald and Manabe*, 1981] with initially saturated soil moisture at irrigation locations to represent irrigation. *Adegoke et al.* [2003] investigated the impact of irrigation on the surface energy budget in the High Plains of the United States using the Colorado State University Regional Atmospheric Modeling System (RAMS [*Pielke et al.*, 1992]) with saturated soil moisture up to a depth of 0.2 m at the beginning of each day in the irrigated locations to represent irrigation. *Boucher et al.* [2004] combined data describing evapotranspiration from irrigation on a country basis with data representing irrigated areas and imported the data set into the general circulation model, LMDZ [e.g., *Zhou and Li*, 2002], with a prescribed artificial source of water vapor equal to the irrigation flux to elucidate the potential impact of irrigation on the global atmosphere. *Lobell et al.* [2006] addressed a potential bias of model-projected greenhouse warming in irrigated regions using the National Center for Atmospheric Researc (NCAR) CAM3 general circulation model (GCM) [*Collins et al.*, 2004] with saturated soil moisture in all agricultural soil columns to represent irrigation. *Kueppers et al.* [2007] found that a regional irrigation cooling effect exits using the regional climate model, RegCM3 [*Pal et al.*, 2007], with an idealized representation of irrigation given by forcing soil moisture to field capacity at all times. However, the irrigation representations mentioned above are not suitable for evaluation of the effects of water transfer on regional climate, especially for water transfer schemes that involve different intensities.

[5] To investigate the effects of interbasin water transfer on regional climate, we developed a water transfer mechanism that accounts for the water to be transferred by increasing the available quantity of water that reaches the surface in the intake areas according to the spatial and temporal distribution schemes of the water transfer. We then implemented the water transfer mechanism into the regional climate model, RegCM3. Specifically, the climatic responses to three water transfer schemes in the Middle Route of the South-to-North Water Transfer Project (MRSNWTP) in China were evaluated in this study.

[6] In section 2 of this paper, the regional climate model, the water transfer mechanism, and the setup of the numerical experiments are described. Section 3 discusses the effects of interbasin water transfer on regional climate. The results of the study are concluded and discussed in section 4.

## 2. Model Description and Experimental Design

### 2.1. Regional Climate Model RegCM3

[7] In this study, RegCM3 was used to evaluate the role of climatic responses of interbasin water transfer. The model was originally developed by the NCAR, and its latest version, which is known as the ICTP Regional Climate Model version 3 (RegCM3), was developed by the Abdus Salam International Centre for Theoretical Physics (ICTP) [*Pal et al.*, 2007]. RegCM3 is a dimensional, hydrostatic, compressible, primitive equation, $\sigma$-vertical coordinate regional climate model. The dynamic core of RegCM3 is based on the hydrostatic version of the fifth-generation Pennsylvania State University/National Center for Atmospheric Research (PSU/NCAR) mesoscale model [*Grell et al.*, 1994]. The model currently employs the radiative transfer package used in the NCAR's Community Climate Model, version 3 (CCM3) [*Kiehl et al.*, 1996]. In addition, land surface physics are modeled by the Biosphere-Atmosphere Transfer Scheme version 1e (BATS1e) developed by *Dickinson et al.* [1993],

while boundary layer physics are modeled using the nonlocal planetary boundary layer scheme developed by *Holtslag et al.* [1990], as described by *Giorgi et al.* [1993a]. RegCM3 also employs the bulk aerodynamic ocean flux parameterization described by *Zeng et al.* [1998], in which sea surface temperatures (SSTs) are prescribed. Three different convection schemes (Kuo, Grell, and Emanuel) are available for the nonresolvable rainfall processes [*Giorgi et al.*, 1993b]. RegCM3 has been validated against observations of modern-day climate in China [*Gao et al.*, 2004; *Zhang et al.*, 2005, 2007; *Yuan et al.*, 2008; *Zheng et al.*, 2009]. Additionally, the model has been found to do a good job of simulating spatial and temporal climate features [*Bell et al.*, 2004; *Gao et al.*, 2001, 2002, 2006, 2008; *Snyder et al.*, 2002].

### 2.2. A Water Transfer Mechanism and Its Implementation in RegCM3

[8] To investigate the climatic responses of interbasin water transfer, we first described the water transfer mechanism. It describes a water source area where water is transferred from, a water receiving area where water is transferred into, and the quantity of water to be transferred at any given time and in a place of an intake area. The water to be transferred is usually taken from reservoirs in the water source area, diverted by transportation channels, and ultimately distributed into the water receiving area. Through water transfer, water is taken directly from a reservoir in a water source area; therefore the land surface conditions in the water source area are not changed as much as those in the water receiving area [*Lin and Peng*, 1986; *Duan et al.*, 1996; *Zhang et al.*, 2004]. Thus we only focused on the climatic responses to the land surface changes from water transfer into a water receiving area in the present study.

[9] The spatial and temporal distributions of irrigation water from the water transfer at a model grid in an intake area were derived according to the water transfer scheme. Water to be transferred into an intake area was treated as increasing the available quantity of water, which was added to the precipitation that reached the surface. It was described as follows:

$$P_{net} = P_r + P_w + S_m - E, \tag{1}$$

where $P_{net}$ is the net water applied to the surface, $P_r$ is rainfall, $P_w$ is the additional water from the water transfer, $S_m$ is snowmelt, and $E$ is evaporation.

[10] The water transfer mechanism was then coupled into the land surface model BATS1e [*Dickinson et al.*, 1993], which is the land surface component of RegCM3. The regional climate model, RegCM3, with the water transfer representation was then used to investigate the climatic responses of interbasin water transfer.

### 2.3. Study Domain and Experimental Design

[11] The Middle Route of the South-to-North Water Transfer Project (MRSNWTP) in China was chosen for this study to investigate the climatic responses to three water transfer schemes with intensities of 7.5, 8.5, and 11.8 billion $m^3$/yr according to the project programming [*Changjiang Water Resources Commission*, 2001b]. As shown in Figure 1, the middle route would transfer water from the Danjiangkou reservoir on the Han River, which is a large tributary to the middle reaches of the Yangtze River, to Hubei, Henan, and Hebei provinces, and ultimately to Beijing and Tianjin, as well as to the western part of the north China Plain [*Liu and Du*, 1985; *Liu and Zheng*, 2002]. The region consisting of the counties shown in Figure 1b is the intake area, and the blue box shown in Figure 1c is Huabei Plain. The total length of the main canal will be approximately 1246 km, with about 482 km being located in the southern portion of the Yellow River and about 764 km being located in the northern portion of the Yellow River [*Liu and Zheng*, 2002]. The water to be transferred along the middle route will flow north via gravity.

[12] The Danjiangkou reservoir has an annual natural inflow of 41.1 billion $m^3$ from a drainage area of 95,217 $km^2$. The first-stage engineering projects include the completed 162 m Danjiangkou dam, which has a total storage capacity of 17.45 billion $m^3$. The second-stage engineering projects will raise the dam to an elevation of 176.6 m to increase the total storage capacity to 29.1 billion $m^3$. The three water transfer schemes evaluated in this study, which had intensities of 7.5, 8.5, and 11.8 billion $m^3$/yr, were developed according to the water demand and supply balance analysis. Specifically, these intensities correspond to the recent demand without the increased dam height (scheme 1), the recent demand with the increase in dam height (scheme 2), and the future demand with the increased dam height (scheme 3) [*Changjiang Water Resources Commission*, 2001b]. The quantity of water to be transferred for schemes 1, 2, and 3 is allocated to each county in the intake area as shown in Table 1.

[13] In the absence of explicit spatial and temporal data, the actual distribution and usage of the water to be transferred by the MRSNWTP is difficult to determine. Therefore we derived the spatial and temporal water transfer data under the assumption that the quantity of water to be transferred to a county in the intake area for a year is distributed evenly into each time step for the year. We believe that this assumption provides a reasonable approximation since the realistic quantity and spatial distribution of the water transfer project are introduced in the study.

[14] On the basis of the derived spatial and temporal water transfer data for the three water schemes of the MRSNWTP mentioned above, four 10-year simulations were conducted, a control run (MCTL) without water transfer, and three water transfer runs MWT1, MWT2, and MWT3 that corresponded to scheme 1, scheme 2, and scheme 3, respectively. We used the domain centered at 36.5°N, 114.5°E, which spanned 24°N to 48°N and 98°E to 131°E, had a horizontal resolution of 30 km and contained 12 grid points as a lateral buffer zone as the simulation domain (Figure 1c). In addition, we used the ERA40 reanalysis data [*Uppala et al.*, 2005] and the National Oceanic and Atmospheric Administration optimally interpolated sea surface temperatures [*Reynolds et al.*, 2002] as lateral boundary conditions. The Grell scheme was chosen for our experiments. All four simulations ran from 1 January 1991 to 31 December 2000. The first year was used for spin-up, and the last 9 years were selected for analysis.

[15] To further discuss the effects of interbasin water transfer and their uncertainties, two additional 10-year water transfer runs (MWT4, MINT) were conducted. Run MWT4

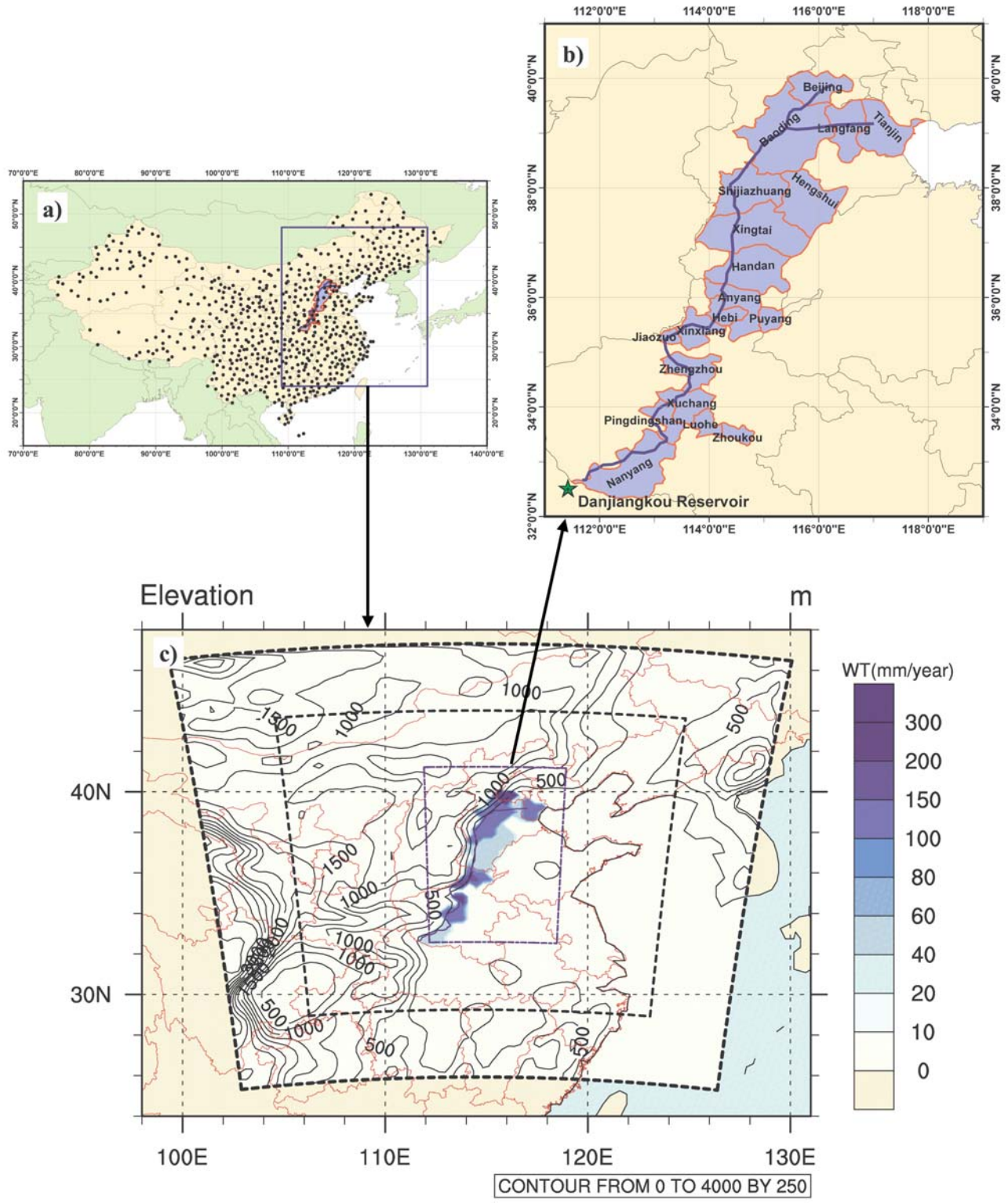


**Figure 1.** The study domain: (a) the location of the study domain; (b) the counties where water is transferred through the Middle Route of the South-to-North Water Transfer Project (MRSNWTP); and (c) the distribution of the annual quantity of water to be transferred for water transfer scheme 3 (contours, elevation; color fill, water transfer quantity). The black dots in Figure 1a represent 753 meteorological stations in China. The counties in Figure 1b are the intake area, and the blue box in Figure 1c is Huabei Plain.

**Table 1.** Water Allocation of the Three Water Transfer Schemes[a]

| Province | County | Scheme 1 | Scheme 2 | Scheme 3 |
|---|---|---|---|---|
| Henan | Diaohe | 4.53 | 5.33 | 5.27 |
| | Nanyang | 2.06 | 2.67 | 5.41 |
| | Luohe | 1.09 | 1.34 | 2.19 |
| | Zhoukou | 1.16 | 1.42 | 1.93 |
| | Pingdingshan | 2.09 | 2.49 | 4.01 |
| | Xuchang | 1.49 | 1.68 | 3.94 |
| | Zhengzhou | 5.68 | 6.74 | 9.29 |
| | Jiaozuo | 2.22 | 2.69 | 3.13 |
| | Xinxiang | 3.58 | 4.35 | 6.51 |
| | Hebi | 2.01 | 2.48 | 3.51 |
| | Puyang | 0.99 | 1.19 | 1.57 |
| | Anyang | 2.70 | 3.38 | 5.68 |
| Hebei | Handan | 2.60 | 3.18 | 4.31 |
| | Xingtai | 3.01 | 3.62 | 4.95 |
| | Shijiazhuang | 6.59 | 7.78 | 10.05 |
| | Hengshui | 2.46 | 3.09 | 4.11 |
| | Baoding | 9.14 | 11.26 | 16.64 |
| | Langfang | 1.21 | 1.47 | 2.23 |
| Beijing | Beijing | 11.20 | 10.52 | 14.87 |
| Tianjing | Tianjing | 9.18 | 8.63 | 8.56 |
| Total | | 75.0 | 85.3 | 118.2 |

[a]Units are $10^8$ $m^3$.

employed the same configuration as run MWT3 and was conducted using the spatial and temporal water transfer data derived from scheme 3 under the assumption that the quantity of water to be transferred to the intake area of a county in a year is distributed evenly into each time step of the first half of the year. In addition, the MINT run was designed to evaluate the model initialization influence on regional climate. The MINT run also used the same configuration as the MWT3 run and was conducted without water transfer from 1 January 1991 to 31 December 1991 but with the water transfer scheme 3 from 1 January 1992 to 31 December 2000.

## 3. Results

### 3.1. Validation of the Control Run (MCTL)

[16] Observations of precipitation and temperature from the 753 meteorological stations in China shown in Figure 1a were used to validate the two important model output variables, precipitation and temperature. The observation data set was obtained through linear interpolation weighted by the inverse squared distances between the gauges and the grid cells [*Xie et al.*, 2007]. In the following analysis of the runs mentioned in section 2.3, we did not consider the effects of the lateral buffer zone (12 grid points, the area between two black dashed sectorial boxes in Figure 1c).

[17] Figure 2 shows the 9-year mean annual precipitation and 2 m mean air temperature over land based on observations and the control run. The simulated precipitation decreased from south to north, which is consistent with the observations. The position of the 800 mm isohyet line from the control run was very similar to that of the observations. However, the magnitude of precipitation from the control run was greater than that of the observations. Additionally, the model performed better for temperature than for precipitation. Specifically, the pattern of the simulated temperature matched well with the observations, although there was an ~1°–2°C cold deviation over north China.

[18] To quantitatively evaluate the model performance, we calculated the spatial correlation coefficient (COR) and standard departure (STD) using the following equations:

$$COR = \frac{\sum_{i=1}^{N}(x_i - \overline{x_i})(x_{io} - \overline{x_{io}})}{\sqrt{\sum_{i=1}^{N}(x_i - \overline{x_i})^2 \sum_{i=1}^{N}(x_{io} - \overline{x_{io}})^2}}, \quad (2)$$

$$STD = \sqrt{\frac{\sum_{i=1}^{N}(x_i - x_{io})^2}{N}}, \quad (3)$$

where $x_i$ ($x_{io}$) is the simulated (observed) value at each grid point, $\overline{x_i}$($\overline{x_{io}}$) is the corresponding mean value of $x_i$ ($x_{io}$) over all grid points and $N$ is the total number of grid points.

[19] The CORs for precipitation and temperature for the model domain excluding the lateral buffer zone were 0.912 and 0.914, where the STDs for those values were 278.9 mm and 2.78°C, respectively. These findings indicate that the RegCM3 simulates the regional climate over the study domain reasonably well.

### 3.2. Effects of Interbasin Water Transfer on Regional Climate

[20] To detect the underlying effects of interbasin water transfer on regional climate, we first discussed the differences in the simulated climate variables induced by water transfer.

[21] Figure 3 shows the differences in the simulation between each water transfer run (MWT1, MWT2, or MWT3) and the control run (MCTL). The average differences over the intake area and the Huabei Plain are shown in Table 2. Over the 9-year time period of the simulated experiments, 74.4, 84.6, and 117.2 mm water was transferred into the intake area for the three water transfer runs, respectively. Most of the water was consumed in enhancing evaporation, and the remainder was translated to additional runoff, soil moisture, and so on. The increases in topsoil moisture and latent heat flux varied as a direct result of injecting water into the intake area. When the three water transfer runs were compared with the control run, increases of 1.3, 1.6, and 2.1 mm in the topsoil moisture, 9.1, 10.3, and 12.0 mm in the total soil moisture, 7.7, 8.9, and 14.9 mm in the surface runoff, and 70.5, 80.9, and 111.9 mm in the evapotranspiration were observed, and these were accompanied by increases of 5.6, 6.4, and 8.9 $W/m^2$, respectively, in the latent heat flux over the intake area. Evaporation of the water to be transferred was also accompanied by cooling of the surface (known as evaporative cooling). The mean annual sensible heat flux decreased by 4.3, 5.1, and 7.0 $W/m^2$ for the three water transfer runs when compared with the control run, respectively, due to decreases in the surface-atmosphere temperature difference. Over the intake area for the three water transfer runs, the 2 m mean air temperature decreased by 0.12°C, 0.15°C, and 0.20°C, the 2 m maximum air temperature decreased by 0.35°C, 0.40°C, and 0.58°C, and the 2 m minimum air temperature decreased by 0.03°C, 0.04°C, and 0.07°C in response to MWT1, MWT2, and MWT3, respectively. In addition, the total precipitation

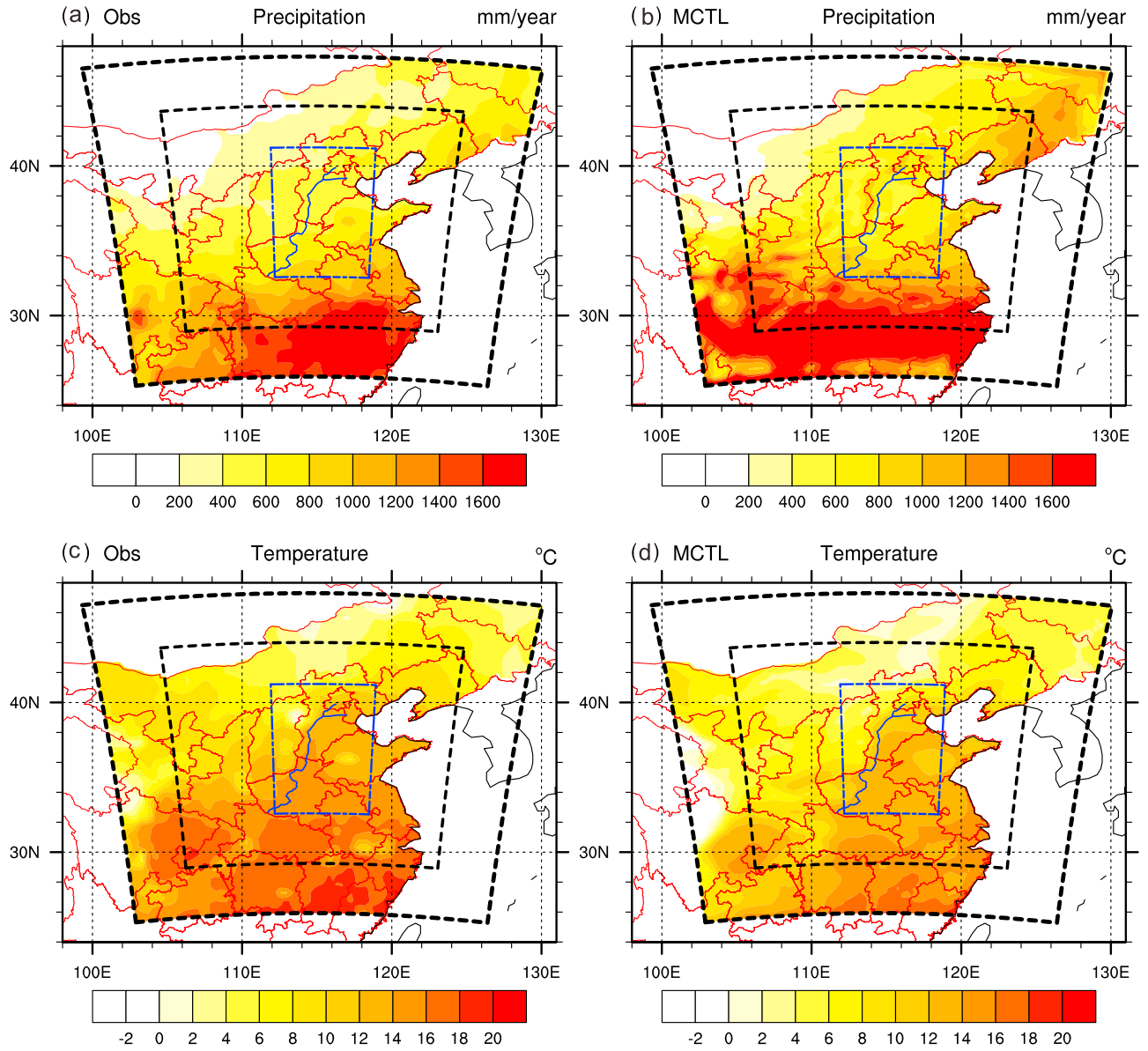


**Figure 2.** The 9-year mean annual precipitation and temperature from (a and c) observed data and (b and d) the control run.

increased by 12.9, 15.5. and 21.6 mm/yr, the convective precipitation increased by 8.6, 9.7, and 16.7 mm/yr, and the large-scale precipitation increased by 4.3, 5.9, and 5.0 mm/yr in MWT1, MWT2, and MWT3, respectively. However, these differences were generally small and statistically insignificant, indicating that the water transfer plays a small role in influencing regional climate in our simulations.

[22] Figure 4 shows the mean monthly differences in 2 m mean air temperature and total precipitation between each water transfer run and the control run over the intake area. The trends in temperature and precipitation differences when compared with the control run were consistent among the three water transfer runs. When compared with the control run, the temperature in the water transfer runs decreased from February to November and increased slightly in December and January, while the total precipitation increased from September to July and decreased slightly in August. It should be noted that the difference in the temperature and precipitation between each water transfer run and the control run had opposite trends. These

**Figure 3.** Annual mean differences between each water transfer run (MWT1, MWT2, and MWT3) and the control run (MCTL) in (a) Pw, annual quantity of water to be transferred, (b) SMT, topsoil moisture, (c) LHFS, latent heat flux, (d) SHFS, sensible heat flux, (e) Tmean, 2 m mean air temperature, (f) Tmax, 2 m maximum air temperature, (g) Tmin, 2 m minimum air temperature, (h) TPR, total precipitation, (i) PRCV, convective precipitation, and (j) PRLS, large-scale precipitation.

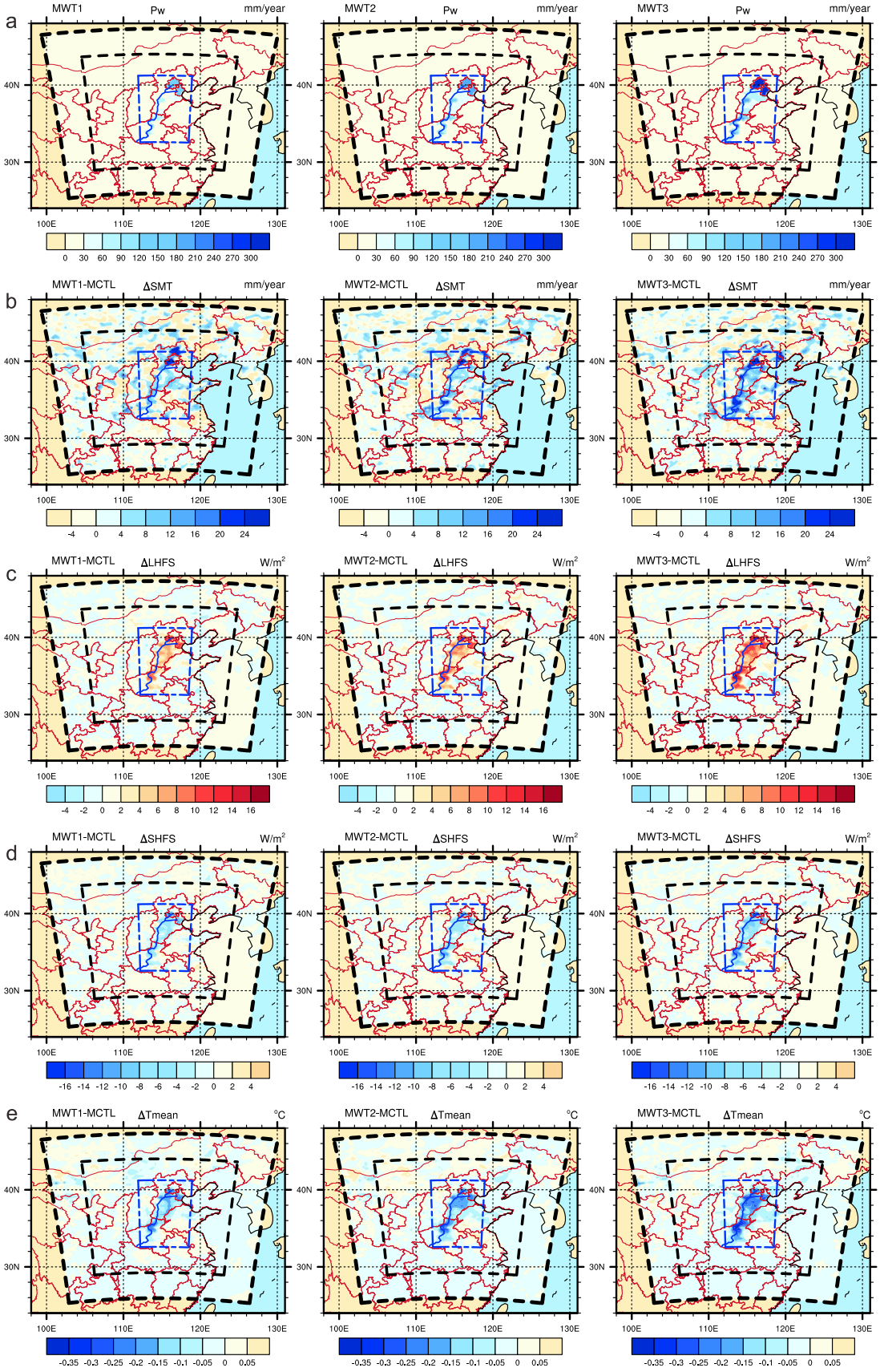
a
MWT1 Pw mm/year
MWT2 Pw mm/year
MWT3 Pw mm/year
0 30 60 90 120 150 180 210 240 270 300
b
MWT1-MCTL ΔSMT mm/year
MWT2-MCTL ΔSMT mm/year
MWT3-MCTL ΔSMT mm/year
-4 0 4 8 12 16 20 24
c
MWT1-MCTL ΔLHFS W/m2
MWT2-MCTL ΔLHFS W/m2
MWT3-MCTL ΔLHFS W/m2
-4 -2 0 2 4 6 8 10 12 14 16
d
MWT1-MCTL ΔSHFS W/m2
MWT2-MCTL ΔSHFS W/m2
MWT3-MCTL ΔSHFS W/m2
-16 -14 -12 -10 -8 -6 -4 -2 0 2 4
e
MWT1-MCTL ΔTmean °C
MWT2-MCTL ΔTmean °C
MWT3-MCTL ΔTmean °C
-0.35 -0.3 -0.25 -0.2 -0.15 -0.1 -0.05 0 0.05
40N
30N
100E 110E 120E 130E

**Figure 3**

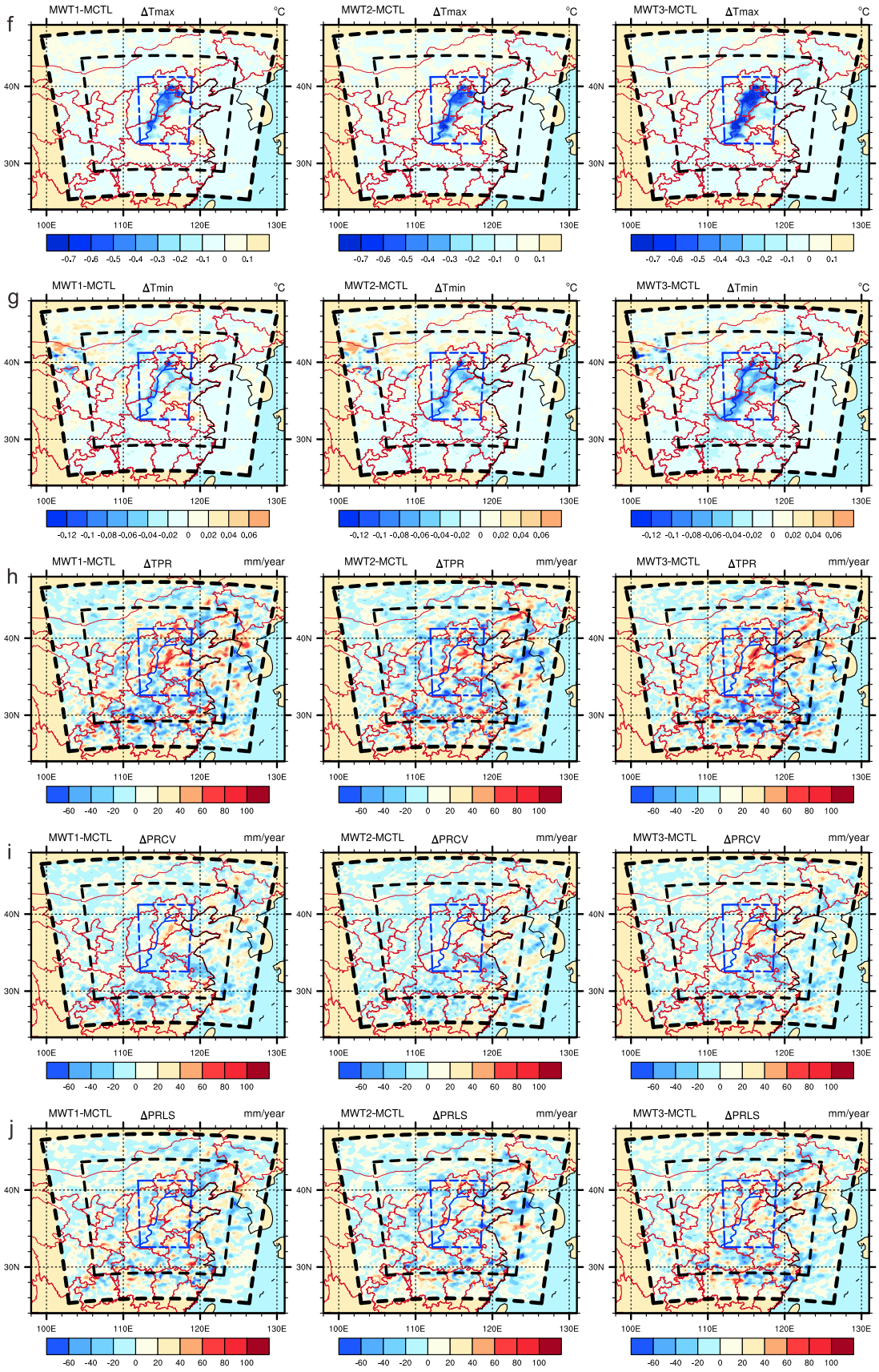


**Figure 3.** (continued)

**Table 2.** Climatic Responses of Different Water Transfer Schemes Over the Intake Area and Huabei Plain[a]

| | MWT1 | | MWT2 | | MWT3 | | MWT4 | |
|---|---|---|---|---|---|---|---|---|
| Variable | Intake | Huabei | Intake | Huabei | Intake | Huabei | Intake | Huabei |
| PW (mm) | 74.4 | 13.0 | 84.6 | 14.8 | 117.2 | 20.5 | 117.2 | 20.5 |
| ΔSCV (mm) | 0.08 | 0.03 | 0.10 | 0.04 | 0.12 | 0.05 | 0.10 | 0.03 |
| ΔSMT (mm) | 1.3 | 0.37 | 1.6 | 0.43 | 2.1 | 0.59 | 1.9 | 0.38 |
| ΔTSW (mm) | 9.1 | −2.7 | 10.3 | −5.2 | 12.0 | −6.9 | 9.6 | 0.56 |
| ΔRunoff (mm) | 7.7 | 3.1 | 8.9 | 1.8 | 14.9 | 4.9 | 14.1 | 1.0 |
| ΔET (mm) | 70.5 | 18.5 | 80.9 | 19.5 | 111.9 | 29.2 | 101.5 | 16.6 |
| ΔLHFS ($W/m^2$) | 5.6 | 1.5 | 6.4 | 1.5 | 8.9 | 2.3 | 8.1 | 1.3 |
| ΔSHFS ($W/m^2$) | −4.3 | −1.0 | −5.1 | −1.1 | −7.0 | −1.7 | −6.7 | −1.0 |
| ΔTmean (°C) | −0.12 | −0.04 | −0.15 | −0.05 | −0.20 | −0.07 | −0.17 | −0.04 |
| ΔTmax (°C) | −0.35 | −0.11 | −0.40 | −0.12 | −0.58 | −0.19 | −0.42 | −0.10 |
| ΔTmin (°C) | −0.03 | −0.02 | −0.04 | −0.02 | −0.07 | −0.03 | −0.03 | −0.01 |
| ΔTPR (mm) | 12.9 | 5.6 | 15.5 | 1.2 | 21.6 | 6.6 | 7.9 | −2.3 |
| ΔPRCV (mm) | 8.6 | 0.98 | 9.7 | −0.46 | 16.7 | 2.7 | 5.3 | −1.7 |
| ΔPRLS (mm) | 4.3 | 4.7 | 5.9 | 1.6 | 5.0 | 3.9 | 2.7 | −0.59 |

[a]Pw, annual quantity of water to be transferred; SCV, snow amount; SMT, top layer (0–10 cm) soil moisture; TSW, total soil moisture; Runoff, surface runoff; ET, evapotranspiration; LHFS, latent heat flux; SHFS, sensible heat flux; Tmean, mean temperature; Tmax, maximum temperature; Tmin, minimum temperature; TPR, total precipitation; PRCV, convective precipitation; PRLS, large-scale precipitation.

findings are consistent with the results of a study conducted by *Chen et al.* [2005]. Despite that the effects of interbasin water transfer were statistically insignificant, those effects would be enhanced when the magnitude and range of the water transfer project increase. (The maximum effects of interbasin water transfer would be found when the soil moisture is forced to saturation due to adequate water is transferred in. The effects would be statistically significant at that moment, as described by *Kueppers et al.* [2007].) The intensity of climatic influences was positively related with the quantity of water to be transferred; however, they do not have a simple linear relationship. Specifically, the climatic responses obtained by scheme 1 of the MWT1 run and scheme 2 of the MWT2 run were not fully consistent, even though the difference in the quantity of the water transferred between the two cases was not large. When compared with the MCTL-run, the mean annual precipitation simulated by the MWT2 run increased by 5.6 mm/yr over the Huabei Plain, while that simulated by MWT1 run increased by only 1.2 mm/yr (see Table 2). This phenomenon can be explained

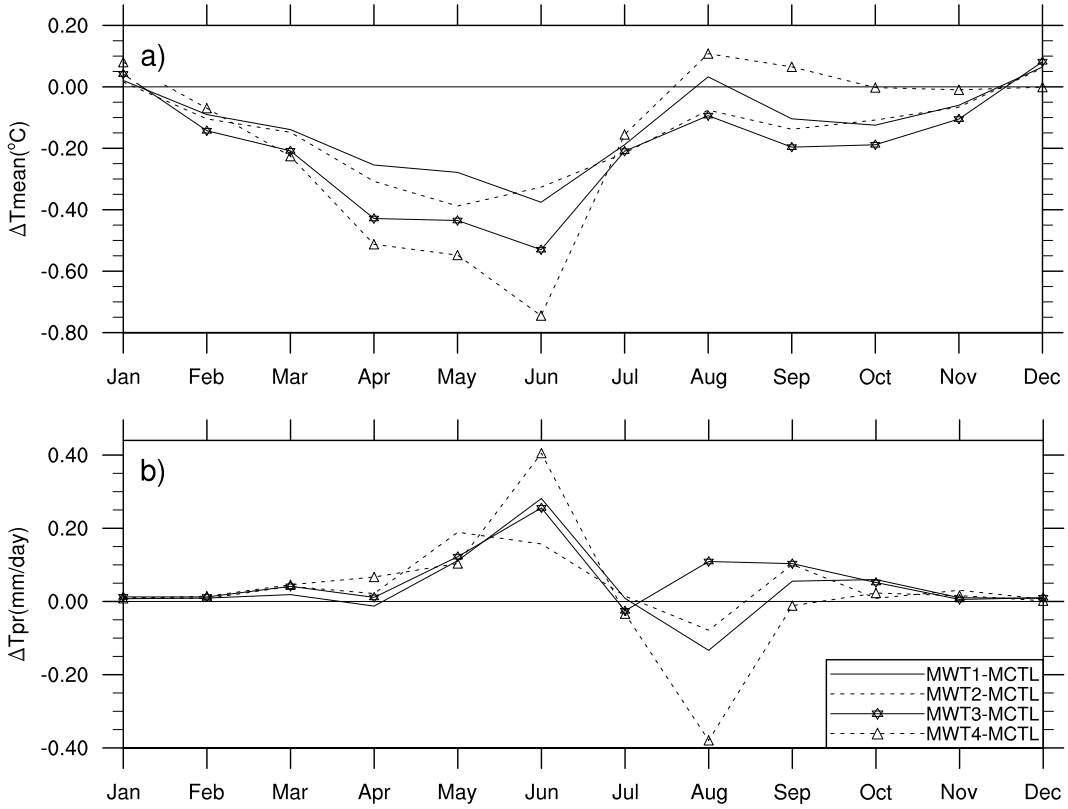


**Figure 4.** The mean monthly temperature and total precipitation differences between each water transfer run (MWT1, MWT2, MWT3, or MWT4) and the control run (MCTL) over the intake area.

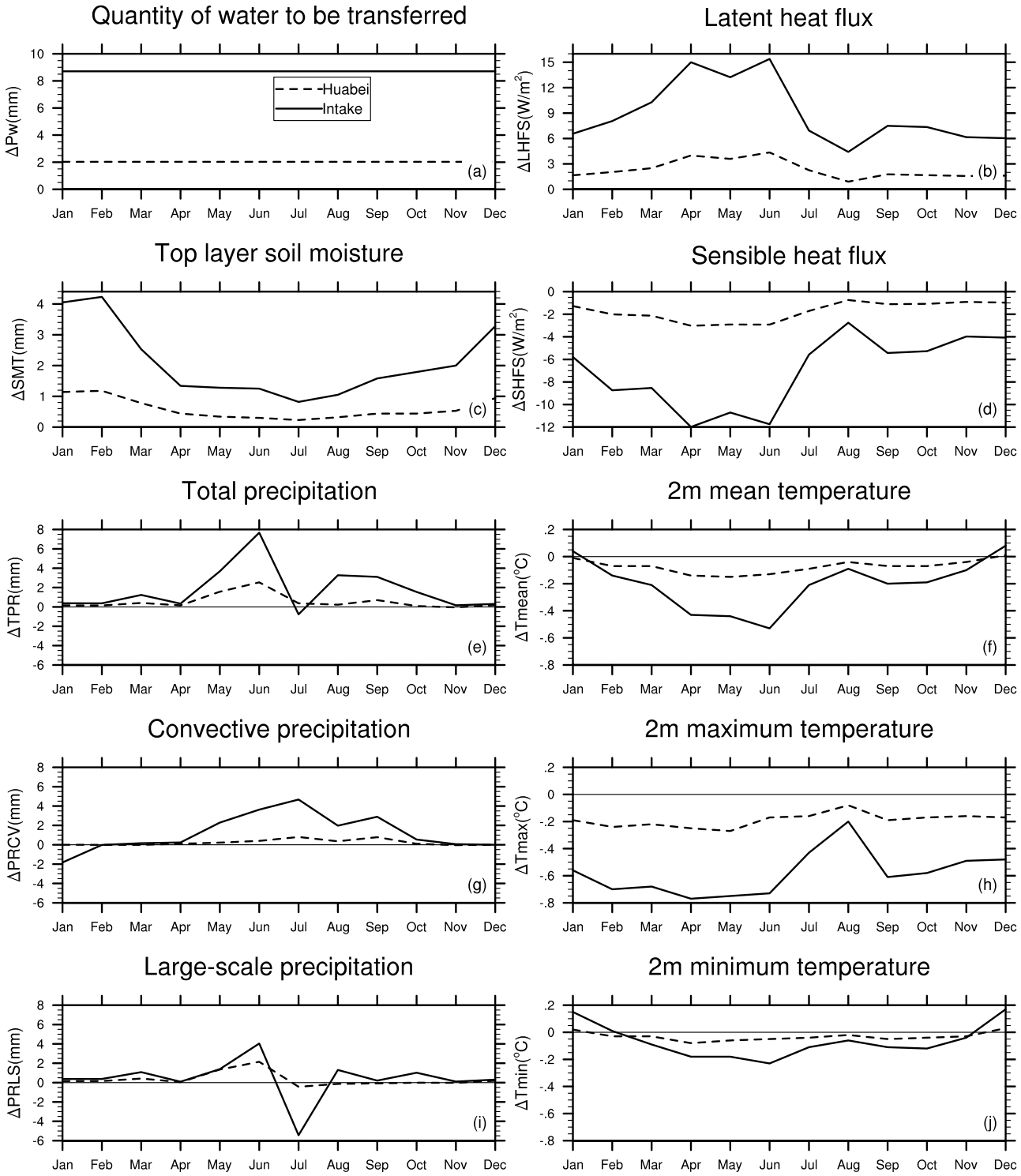


**Figure 5.** Mean monthly climate differences between runs MWT3 and MCTL over the intake area and Huabei Plain. Pw, quantity of water to be transferred; SMT, top layer (0–10 cm) soil moisture; LHFS, latent heat flux; SHFS, sensible heat flux; Tmean, mean temperature; Tmax, maximum temperature; Tmin, minimum temperature; TPR, total precipitation; PRCV, convective precipitation; and PRLS, large-scale precipitation.

**Table 3.** Climate Differences Between Runs MWT3 and MCTL Over the Intake Area and Huabei Plain

| | ΔSMT (mm) | | ΔLHFS (W/m$^2$) | | ΔSHFS (W/m$^2$) | | ΔTmean (°C) | | ΔTmax (°C) | | ΔTmin (°C) | | ΔTPR (mm) | | ΔPRCV (mm) | | ΔPRLS (mm) | |
|---|---|---|---|---|---|---|---|---|---|---|---|---|---|---|---|---|---|---|
| Month | Intake | Huabei | Intake | Huabei | Intake | Huabei | Intake | Huabei | Intake | Huabei | Intake | Huabei | Intake | Huabei | Intake | Huabei | Intake | Huabei |
| Jan | 4.1 | 1.1 | 6.6 | 1.7 | −5.8 | −1.3 | 0.04 | −0.01 | −0.56 | −0.19 | 0.15 | 0.02 | 0.38 | 0.16 | −1.8 | 0.00 | 0.38 | 0.16 |
| Feb | 4.2 | 1.2 | 8.1 | 2.0 | −8.7 | −2.0 | −0.14 | −0.07 | −0.70 | −0.24 | 0.01 | −0.03 | 0.37 | 0.15 | −0.02 | −0.01 | 0.38 | 0.16 |
| Mar | 2.5 | 0.78 | 10.3 | 2.5 | −8.5 | −2.1 | −0.21 | −0.07 | −0.68 | −0.22 | −0.09 | −0.03 | 1.2 | 0.41 | 0.16 | −0.01 | 1.1 | 0.42 |
| Apr | 1.3 | 0.44 | 15.0 | 4.0 | −12.0 | −3.0 | −0.43 | −0.14 | −0.77 | −0.25 | −0.18 | −0.08 | 0.34 | 0.16 | 0.24 | 0.10 | 0.09 | 0.05 |
| May | 1.3 | 0.34 | 13.2 | 3.6 | −10.7 | −2.9 | −0.44 | −0.15 | −0.75 | −0.27 | −0.18 | −0.06 | 3.7 | 1.6 | 2.3 | 0.22 | 1.4 | 1.4 |
| Jun | 1.3 | 0.30 | 15.4 | 4.4 | −11.7 | −2.9 | −0.53 | −0.13 | −0.73 | −0.17 | −0.23 | −0.05 | 7.7 | 2.5 | 3.6 | 0.40 | 4.0 | 2.2 |
| Jul | 0.82 | 0.23 | 6.9 | 2.3 | −5.6 | −1.7 | −0.21 | −0.09 | −0.43 | −0.16 | −0.11 | −0.04 | −0.77 | 0.37 | 4.7 | 0.80 | −5.4 | −0.43 |
| Aug | 1.1 | 0.32 | 4.4 | 0.9 | −2.8 | −0.74 | −0.09 | −0.04 | −0.20 | −0.08 | −0.06 | −0.02 | 3.3 | 0.23 | 2.0 | 0.36 | 1.3 | −0.13 |
| Sep | 1.6 | 0.44 | 7.5 | 1.8 | −5.4 | −1.1 | −0.20 | −0.07 | −0.61 | −0.19 | −0.11 | −0.05 | 3.1 | 0.70 | 2.9 | 0.78 | 0.21 | −0.08 |
| Oct | 1.8 | 0.44 | 7.4 | 1.7 | −5.3 | −1.1 | −0.19 | −0.07 | −0.58 | −0.17 | −0.12 | −0.04 | 1.6 | 0.09 | 0.54 | 0.10 | 1.0 | −0.01 |
| Nov | 2.0 | 0.53 | 6.2 | 1.6 | −4.0 | −0.91 | −0.10 | −0.04 | −0.49 | −0.16 | −0.04 | −0.03 | 0.17 | −0.05 | 0.06 | −0.04 | 0.11 | −0.02 |
| Dec | 3.3 | 0.94 | 6.0 | 1.6 | −4.1 | −0.97 | 0.08 | 0.01 | −0.48 | −0.17 | 0.17 | 0.03 | 0.31 | 0.19 | 0.00 | 0.00 | 0.31 | 0.19 |
| Annual | 2.1 | 0.59 | 8.9 | 2.3 | −7.1 | −1.7 | −0.20 | −0.07 | −0.58 | −0.19 | −0.07 | −0.03 | 21.3 | 6.5 | 14.6 | 2.7 | 4.9 | 3.8 |
| Corr[a] | … | **0.97** | … | **0.90** | … | **0.91** | … | **0.76** | … | **0.81** | … | **0.50** | … | **0.13** | … | **0.19** | … | 0.03 |

[a]Corr indicates the spatial correlation coefficient between variable and water transfer distribution (bold values indicate the spatial correlation had statistically significant ($p < 0.05$) between the change of the variable and the quantity of the water to be transferred).

by the difference in spatial distribution in the water to be transferred and the complex general circulation of the atmosphere.

[23] As shown in Table 2, the simulated results obtained during runs MWT3 and MWT4 with the same intensity of water under different water distribution assumptions were similar and produced little difference in the magnitude of the annual climatic responses. The differences in seasonal climatic responses between the two runs are shown in Figure 4. When run MWT4 was compared with run MWT3, an obviously larger decrease in temperature and increase in precipitation were observed during the first half of the year. This difference occurred because the intensity of water transferred per unit of time in run MWT4 was double that of run MWT3. In the second half year, a slight increase in temperature from August to September and a deep decrease in precipitation in August were observed because no water was transferred during that period. These findings demonstrate that the temporal distribution of the water to be transferred has the same impact as intensity on the effects of interbasin water transfer on regional climate.

[24] To further investigate the effects of the interbasin water transfer on regional climate, scheme 3 related to run MWT3 was taken as an example. Figure 5 shows the mean monthly differences in climate between runs MWT3 and MCTL over the intake area and Huabei Plain. The difference in the topsoil moisture between the two runs changed greatly. This change was especially noticeable during the winter months due to low precipitation in winter. However, the largest climatic response (changes in latent heat flux, sensible heat flux, 2 m air mean/maximum/minimum temperatures, total/convective/large-scale precipitation) in a year was observed during spring and the early summer. This was because there is low soil moisture during this period, which can be changed significantly by the transferred water, and the needed energy for evaporation is enough. For example, the mean, maximum, and minimum temperatures in the intake area showed the largest decreases of 0.53°C, 0.73°C, and 0.23°C in June, respectively, while they increased slightly during winter months (Table 3). On the basis of these results, it can be inferred that the seasonal temperature range decreases due to the decrease in temperature in summer and the increase in temperature in winter. The total, convective, and large-scale precipitation increased slightly over both the intake area and Huabei Plain during most months, especially June. The greatest change in the annual precipitation over the intake area was in convective precipitation, while that over the no-intake area of the Huabei Plain was in large-scale precipitation. This indicates that water transfer may primarily influence precipitation by changing the convective precipitation over the intake area and the large-scale precipitation over other adjacent regions. However, more studies are needed to validate this inference. The spatial relationship between water transfer and its climatic responses is a noteworthy question. On the basis of the information shown in Figure 3, the minimum temperature does not change as obviously as the mean and maximum temperatures and is less geographically consistent with the distribution of the transferred water than the mean and maximum temperatures. The spatial correlation coefficient between the changes of variables and the quantity of the transferred water over the Huabei Plain is also shown in

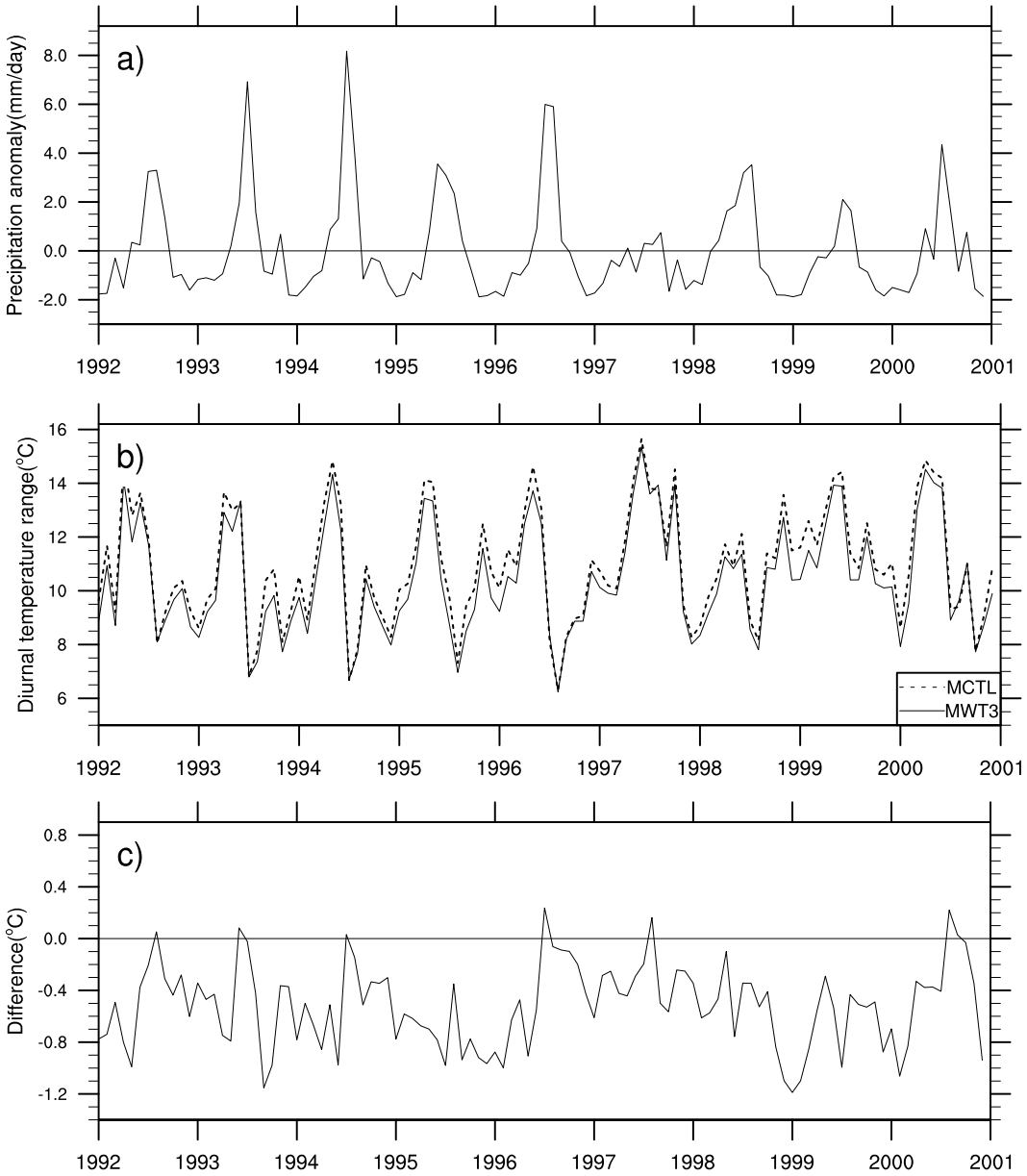


**Figure 6.** From January 1992 to December 2000, (a) monthly mean precipitation deviations from the 1992–2000 monthly means; (b) monthly mean diurnal temperature range simulated by runs MCTL and MWT3; and (c) the difference between the monthly mean diurnal temperature range between both cases.

Table 3 (see the CORR row). The changes in topsoil moisture, latent heat flux, sensible heat flux, and temperature were geographically consistent with the water transfer distribution, while the changes in precipitation were not as obvious. However, all of the variables except for the large-scale precipitation differed significantly ($p < 0.05$) between run MWT3 and MCTL.

[25] The water transfer also reduced the diurnal temperature range (Figures 6b and 6c). From year to year, the change in the diurnal temperature range was influenced by precipitation because the range of the decrease was partially dependent on the available soil moisture used for evapotranspiration, which is primarily determined by the precipitation over the previous 2 months. Indeed, the change in the diurnal temperature range was positively related to the precipitation during the previous 2 months over all of the years evaluated ($r = 0.48$, $n = 108$) (Figures 6a and 6c).

[26] Furthermore, water transfer not only decreased the temperature in the intake grid cells, but also impacted the temperature in their adjacent grid cells and decreases in the temperature of the troposphere via air convection. As shown in Table 3, the mean annual 2 m air temperature over the entire Huabei Plain decreased by 0.07°C. Although the decreases in temperature outside of the intake area were not as obvious as those in the intake area, the decreases diffused over almost the entire Huabei Plain. Figure 7a shows the changes in the vertical profile of the simulated mean air temperature over the intake area and Huabei Plain. The

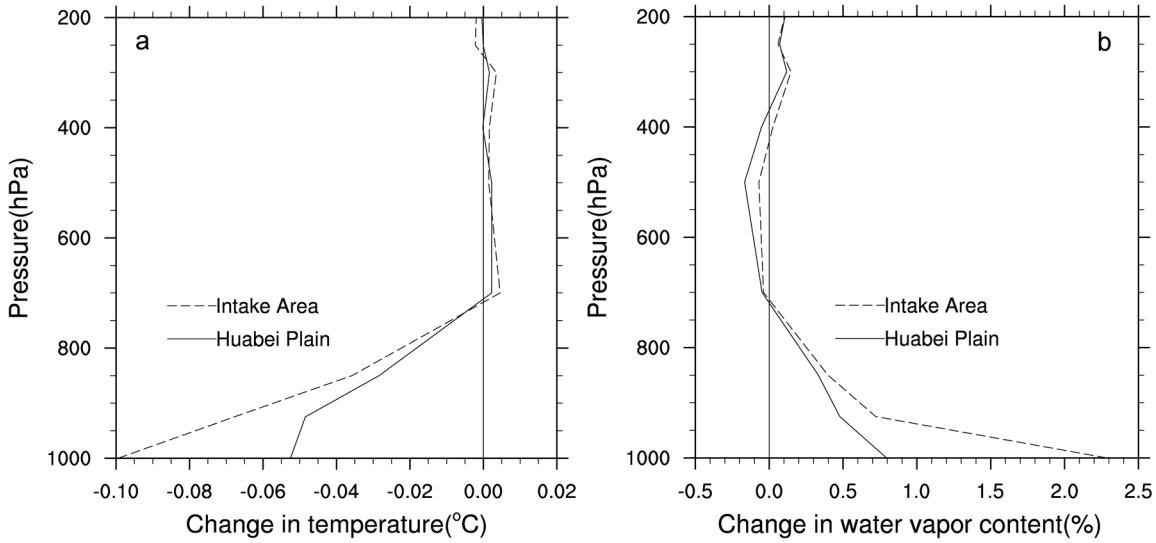


**Figure 7.** Change in the vertical profile of (a) temperature (expressed as a difference in temperature in °C) and (b) water vapor content (expressed in % change of water vapor content in kg/kg), between runs MWT3 and MCTL. For each plot we show the average for the intake area (dashed line) and Huabei Plain (solid line).

temperature at below 700 hPa decreased, while the temperature between 400 and 700 hPa increased slightly. Evaporation of the water to be transferred was accompanied with a cooling of the surface. The additional water vapor injected into the atmosphere will eventually condense, which will release latent heat in the atmosphere, thereby heating and drying the atmosphere between 400 and 700 hPa (see Figure 7b). Therefore the water transfer will also have a direct effect on the temperature profile by cooling the surface and heating the atmosphere.

[27] In addition, the regional circulation changed due to transfer of water into the intake area. The contour map in Figure 8 shows the vertical cross section of the difference in the modeled easterly wind velocity (decreases with dashed contours and increases with solid contours) between runs MWT3 and MCTL along a line of constant latitude (40.0°N). Because of the discrepancy between land-sea and topography, the near-surface temperature was relatively high over the intake area toward the eastward grid cells and relatively low over the intake area toward the westward grid cells. The decrease in near-surface temperature in the intake area reduced the temperature contrast between intake grid cells and sea grid cells on the east side, while it enhanced the contrast between the relatively cool, wet intake grid cells and adjacent warm, dry grid cells on the west side. This led to a weakening wind velocity of the easterly breeze by 2 to 6 cm/s from 119°E to 125°E, and 2 to 5 cm/s from 113°E to 115°E.

[28] The increased evaporation was also accompanied by a change in water vapor. As shown in Figure 7b, a regional increase in water vapor content (which is highest close to the surface) and a slight decrease between 400 and 700 hPa was predicted over the intake area and Huabei Plain. Such changes may enhance the local convection and lead to more convective precipitation.

[29] To investigate the effects of interbasin water transfer on macroscale and mesoscale atmospheric processes, the atmospheric moisture budgets in Huabei Plain were analyzed. Following the definitions of *Schar et al.* [1999], the balance equation for the atmospheric moisture can be written as follows:

$$\Delta W = q_{in} - q_{out} + ET_b - P_b, \tag{4}$$

where $\Delta W$ (mm/d) denotes the tendency of the atmospheric water content during the integration period; $q_{in}$ (mm/d) and $q_{out}$ (mm/d) denote the 9-year mean water flux into and out of the domain, respectively; and $ET_b$ (mm/d) and $P_b$ (mm/d) are the 9-year mean evapotranspiration and precipitation in the domain, respectively. In this study, the adopted averaging was based on 24-h output data. A comparison of the results obtained using shorter averaging periods (down to 3 h) confirmed that an output interval of 24 h was sufficient for the purposes of this study. Nevertheless, the procedure produced some small errors, which implies that the budget relationship (4) is only approximately satisfied. Therefore, for internal consistency, we corrected the atmospheric fluxes $q_{in}$ and $q_{out}$ to fully satisfy the budget constraints (4). The correction was as follows:

$$q_{in}^{corr} = q_{in} - \varepsilon/2,\ q_{out}^{corr} = q_{out} + \varepsilon/2, \tag{5}$$

where $\varepsilon$ is residual water for the imbalance, which can be computed by

$$\varepsilon = q_{in} - q_{out} + ET_b - P - \Delta W. \tag{6}$$

The corrected fluxes fully satisfied the budget constraint.

[30] Figure 9 shows the atmospheric water budgets for runs MCTL and MWT3, and the difference between them. The simulated precipitation and evaporation in run MWT3 were higher than in run MCTL, and the difference in the precipitation between the two runs and that of the evaporation was 6.6 mm/yr and 29.2 mm/yr, respectively. Additionally, the trend in moisture convergence ($MC = q_{in} - q_{out}$)

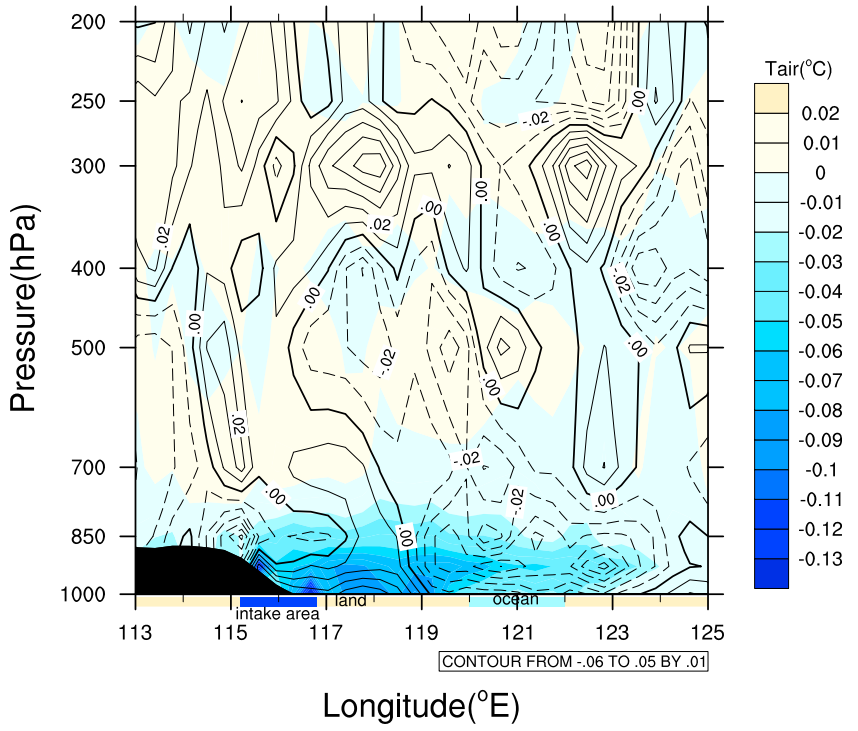


**Figure 8.** Vertical cross section of the modeled atmospheric temperature difference (color fill) and easterly wind velocity difference (decreases with dashed contours and increases with solid contours) between runs MWT3 and MCTL along a line of constant latitude (40.0°N). The longitudinal extent of the intake grid, land grid, and ocean grid is shown with blue, light yellow, and light blue boxes below the *x* axis, respectively. The black irregular graph at the bottom of the figure is the land surface.

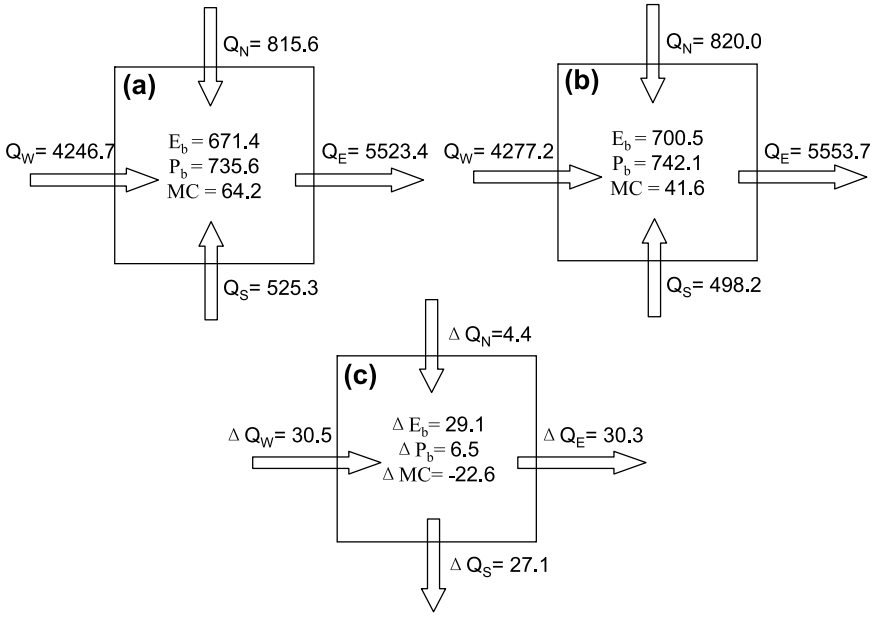


**Figure 9.** Atmospheric water budget diagram for (a) MCTL run, (b) MWT3 run, and (c) their difference (MWT3 − MCTL). *E* and *P* indicate evaporation and precipitation. Arrows indicate incoming and outgoing zonal and meridional moisture flux, respectively. Each numeral denotes the average amount for all grid cells within Huabei Plain; units are mm/yr.

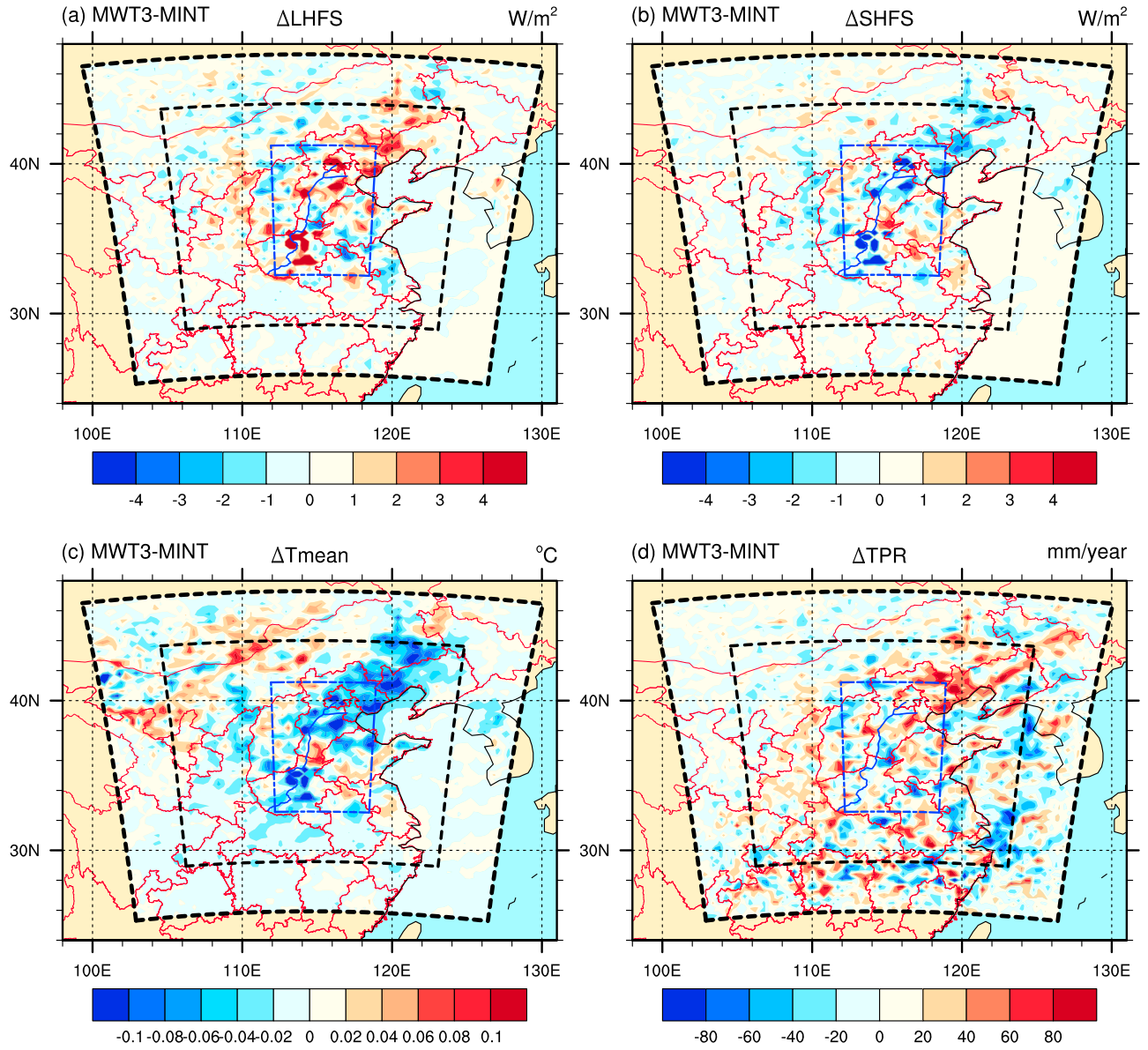


**Figure 10.** The 9-year mean differences between runs MWT3 and MINT in (a) LHFS, latent heat flux, (b) SHFS, sensible heat flux, (c) Tmean, 2 m mean air temperature, (d) TPR, total precipitation.

was opposite to that of the precipitation and evaporation, as indicated by a decrease of 22.6 mm/yr. These findings indicate that water transfer will not only affect the local climate, but also the regional climate by changing the water vapor transport.

### 3.3. Uncertainty in the Model Initialization

[31] To investigate the effects of soil moisture and temperature initialization on the simulations, we used the first year with or without water transfer scheme implemented as a spin-up period. Figure 10 shows the different climatic responses between run MWT3 with a 1-year spin-up period and run MINT without the spin-up period. The differences between the two simulations due to the model initialization primarily appeared in the middle of the study domain, while the differences in the 2 m mean air temperature and precipitation extended to the surrounding area. However, the magnitudes of the differences were all small. When considering the model initialization, the topsoil moisture and latent heat flux increased by 0.06 mm, 0.09 W/m$^2$, while the sensible heat flux, 2 m mean air temperature, and precipitation respectively decreased by 0.12 W/m$^2$, 0.02°C, and 4.0 mm/yr over the intake area. These findings indicate that the uncertainty of the effects of model initialization on the climatic response are finite and the RegCM3 with water transfer scheme can be used to investigate the effects of interbasin water transfer on regional climate over the study domain.

## 4. Discussion and Conclusions

[32] In this study, a water transfer mechanism was implemented into the regional climate model, RegCM3, which represents water to be transferred by increasing the available quantity of water that reaches the surface in intake areas.

The climatic responses of the Middle Route of the South-to-North Water Transfer Project were then investigated using RegCM3 based on the three water transfer schemes of the project. The results indicated that the water transfer should change the local evapotranspiration via an increase in the soil moisture and cause local temperature and precipitation changes by changing the surface water and energy balances. Furthermore, the results suggested that local changes will cause the atmospheric circulation to change and affect the regional climate over adjacent grid cells. Over all of the years evaluated, the magnitude of climatic responses was found to depend on the intensity and spatial and temporal distribution of the water transfer scheme. Furthermore, the effects of the water transfer were found to be larger in spring and autumn than in summer and winter. These differences likely occurred because there is not enough energy in winter to evaporate the transferred water, while there is enough water in summer for evaporation to occur prior to transfer.

[33] The simulations also indicated that water transfer can cause decreases in the seasonal and diurnal temperature ranges, and increases in local precipitation. Therefore the MRSNWTP will not only alleviate the water shortages in north China but also improve the local drought climate environment to some extent. Specifically, the results suggest that the MRSNWTP will be beneficial for the regional ecological environmental positive circulating and sustainable development. However, this result depends on the model and the treatment of water transfer in the model; therefore more studies are needed to validate the results.

[34] Additionally, it should be noted that there are some uncertainties regarding the actual magnitude of the effects of interbasin water transfer on regional climate. The treatment method used for the interbasin water transfer was an idealized representation due to the lack of actual information. Additionally, although it is widely used throughout the world, RegCM3 has been found to have relatively high sensitivity to soil moisture [*Kueppers et al.*, 2007; *Lobell et al.*, 2008]. In addition, the simulated results produced by the model have been shown to be heavily influenced by internal variability [*Giorgi and Bi*, 2000], and it has been found to underestimate temperatures and overestimate precipitation in north China [*Zhang et al.*, 2007; *Zheng et al.*, 2009]. Furthermore, the dependence on the parameterizations and the assumptions regarding the water transfer in the model imply that more studies are needed to validate the results obtained here. Finally, although the differences caused by interbasin water transfer were not found to be statistically significant, it should be a climate response to a certain extent. Despite these limitations, we believe that the climatic responses of water transfer provided here are qualitatively correct and will be enhanced when the magnitude and range of the project increase.

[35] **Acknowledgments.** The authors would like to thank X. J. Tian, J. Zheng, and X. Yuan for their assistance in model operation and result discussions. This manuscript benefited significantly from the comments and suggestions of the editor, Steve Ghan, and the three anonymous reviewers. This study was supported by the National Basic Research Program under grants 2010CB428403 and 2009CB421407, the Knowledge Innovation Project of the Chinese Academy of Sciences under grant KZCX2-YW-126-2, and the National Natural Science Foundation of China under grant 40821092.

## References

Adegoke, J. O., R. A. Pielke, J. Eastman, R. Mahmood, and K. G. Hubbard (2003), Impact of irrigation on midsummer surface fluxes and temperature under dry synoptic conditions: A regional atmospheric model study of the U.S. High Plains, *Mon. Weather Rev.*, *131*, 556–564, doi:10.1175/1520-0493(2003)131<0556:IOIOMS>2.0.CO;2.

Bell, J. L., L. C. Sloan, and M. A. Snyder (2004), Regional changes in extreme climatic events: A future climate scenario, *J. Clim.*, *17*, 81–87, doi:10.1175/1520-0442(2004)017<0081:RCIECE>2.0.CO;2.

Bonfils, C., and D. Lobell (2007), Empirical evidence for a recent slowdown in irrigation-induced cooling, *Proc. Natl. Acad. Sci. U. S. A.*, *104*(34), 13,582–13,587, doi:10.1073/pnas.0700144104.

Boucher, O., G. Myhre, and A. Myhre (2004), Direct human influence of irrigation on atmospheric water vapour and climate, *Clim. Dyn.*, *22*, 597–603, doi:10.1007/s00382-004-0402-4.

Changjiang Water Resources Commission (2001a), General planning, in *Project Programming of the Middle Route of South-to-North Water Transfer Project* (in Chinese), technical report, 210 pp., Wuhan, China.

Changjiang Water Resources Commission (2001b), Special subject 2: Water supply dispatch and of regulation, in *Project Programming of the Middle Route of South-to-North Water Transfer Project* (in Chinese), technical report,Wuhan, China.

Chen, X., M. Zhao, and J. Zhang (2005), Potential impact of south to north water transferring on the drought in northern China (in Chinese), *Adv. Earth Sci.*, *20*(8), 849–855.

Collins, W. D., et al. (2004), Description of the NCAR community atmosphere model (CAM 3. 0), *Tech. Note NCAR/TN-464+STR*, Natl. Cent. for Atmos. Res., Boulder, Colo.

Dickinson, R., A. Henderson-Sellers, and P. Kennedy (1993), Biosphere Atmosphere Transfer Scheme (BATS) version 1e as coupled to the NCAR Community Climate Model, *Tech. Note NCAR/TN-387 STR*, 72 pp., Natl. Cent. for Atmos. Res., Boulder, Colo.

Duan, D. Y., B. P. Fu, H. Wang, M. N. Zhang, Z. C. Zhu, and G. Y. Luo (1996), Effects of China Three Gorges project on climate and their countermeasure (in Chinese), *J. Nat. Sci. Hunan Normal Univ.*, *19*(1), 87–92.

Gao, X. J., et al. (2001), Climate change due to greenhouse effects in China as simulated by a regional climate model, *Adv. Atmos. Sci.*, *18*, 1224–1230, doi:10.1007/s00376-001-0036-y.

Gao, X. J., Z. C. Zhao, and F. Giorgi (2002), Changes of extreme events in regional climate simulations over East Asia, *Adv. Atmos. Sci.*, *19*, 927–942, doi:10.1007/s00376-002-0056-2.

Gao, X. J., et al. (2004), Simulation of climate and short-term climate prediction in China by CCM3 driven by observed SST, *Chin. J. Atmos. Sci.*, *28*, 63–76.

Gao, X. J., J. S. Pal, and F. Giorgi (2006), Projected changes in mean and extreme precipitation over the Mediterranean region from a high-resolution double nested RCM simulation, *Geophys. Res. Lett.*, *33*, L03706, doi:10.1029/2005GL024954.

Gao, X. J., Y. Shi, R. Song, F. Giorgi, Y. Wang, and D. Zhang (2008), Reduction of future monsoon precipitation over China: Comparison between a high resolution RCM simulation and the driving GCM, *Meteorol. Atmos. Phys.*, *100*, 73–86, doi:10.1007/s00703-008-0296-5.

Giorgi, F., and X. Bi (2000), A study of internal variability of a regional climate model, *J. Geophys. Res.*, *105*, 29,503–29,521, doi:10.1029/2000JD900269.

Giorgi, F., M. Marinucci, and G. Bates (1993a), Development of a second-generation regional climate model (RegCM2): part I. Boundary-layer and radiative transfer processes, *Mon. Weather Rev.*, *121*, 2794–2813, doi:10.1175/1520-0493(1993)121<2794:DOASGR>2.0.CO;2.

Giorgi, F., M. Marinucci, G. Bates, and G. De Canio (1993b), Development of a second-generation regional climate model (RegCM2): part II. Convective processes and assimilation of lateral boundary conditions, *Mon. Weather Rev.*, *121*, 2814–2832, doi:10.1175/1520-0493(1993)121<2814:DOASGR>2.0.CO;2.

Grell, G., J. J. Dudhia, and D. Stauffer (1994), A description of the fifth-generation Penn State/NCAR Mesoscale Model (MM5), *Tech. Note TN-398 STR*, 138 pp., Natl. Cent. for Atmos. Res., Boulder, Colo.

Holtslag, A., E. de Bruijn, and H. Pan (1990), A high-resolution air mass transformation model for short-range weather forecasting, *Mon. Weather Rev.*, *118*, 1561–1575, doi:10.1175/1520-0493(1990)118<1561:AHRAMT>2.0.CO;2.

Kiehl, J., J. Hack, G. Bonan, B. Boville, B. Breigleb, D. Williamson, and P. J. Rasch (1996), Description of the NCAR Community Climate Model (CCM3), *Tech. Note TN-420 STR*, 152 pp., Natl. Cent. for Atmos. Res., Boulder, Colo. (Available at http://www.cgd.ucar.edu/cms/ccm3/TN-420/)

Kueppers, L. M., M. A. Snyder, and L. C. Sloan (2007), Irrigation cooling effect: Regional climate forcing by land-use change, *Geophys. Res. Lett.*, *34*, L03703, doi:10.1029/2006GL028679.

Li, H. Z., Z. Z. Chen, and Z. M. Zeng (1980), A preliminary discussion of the potential effects of the irrigation in the East Route of South-to-North Water Transfer Project on regional climate (in Chinese), *Chin. Sci. Bull.*, *11*, 505–508.

Lin, W. P., and B. Peng (1986), Effects of large water conservancy works on environment in the Beijing-Tianjin area: Miyun and Guanting reservoirs as examples, *Acta Sci. Circumstantiae*, *6*(4), 403–411.

Liu, C. M. (1994), South-to-north water transfer in China, *Chin. Environ. Dev.*, *5*(2), 1–15.

Liu, C. M., and W. Du (1985), A geographic systems analysis on water balance along the eastern route of south-to-north water transfer project for the transfer of Chang River water, *Geogr. Res.*, *4*(3), 81–88.

Liu, C. M., and H. X. Zheng (2002), South-to-north water transfer schemes for China, *Water Resour. Dev.*, *18*(3), 453–471, doi:10.1080/0790062022000006934.

Lobell, D. B., G. Bala, C. Bonfils, and P. B. Duffy (2006), Potential bias of model projected greenhouse warming in irrigated regions, *Geophys. Res. Lett.*, *33*, L13709, doi:10.1029/2006GL026770.

Lobell, D. B., C. J. Bonfils, L. M. Kueppers, and M. A. Snyder (2008), Irrigation cooling effect on temperature and heat index extremes, *Geophys. Res. Lett.*, *35*, L09705, doi:10.1029/2008GL034145.

Manabe, S., and R. J. Stouffer (1980), Sensitivity of a global climate model to an increase of $CO_2$ concentration in the atmosphere, *J. Geophys. Res.*, *85*, 5529–5554, doi:10.1029/JC085iC10p05529.

Pal, J. S., et al. (2007), Regional climate modeling for the developing world: The ICTP RegCM3 and RegCNET, *Bull. Am. Meteorol. Soc.*, *88*, 1395–1409, doi:10.1175/BAMS-88-9-1395.

Pielke, R. A., et al. (1992), A comprehensive meteorological modeling system—RAMS, *Meteorol. Atmos. Phys.*, *49*, 69–91, doi:10.1007/BF01025401.

Pielke, R. A., et al. (2002), The influence of land-use change and landscape dynamics on the climate system—Relevance to climate change policy beyond the radioactive effect of greenhouse gases, *Philos. Trans. R. Soc. London, Ser. A*, *360*, 1705–1719, doi:10.1098/rsta.2002.1027.

Reynolds, R. W., N. A. Rayner, T. M. Smith, D. C. Stokes, and W. Wang (2002), An improved in situ and satellite SST analysis for climate, *J. Clim.*, *15*, 1609–1625, doi:10.1175/1520-0442(2002)015<1609:AIISAS>2.0.CO;2.

Schar, C., et al. (1999), The soil-precipitation feedback: A process study with a regional climate model, *J. Clim.*, *12*, 722–741, doi:10.1175/1520-0442(1999)012<0722:TSPFAP>2.0.CO;2.

Shan, F., X. L. Ling, G. D. Zhi, and L. Z. Jin (2007), Assessing the impacts of South-to-North Water Transfer Project with decision support systems, *Decis. Support Syst. Emerging Econ.*, *42*(4), 1989–2003.

Snyder, M. A., J. L. Bell, L. C. Sloan, P. B. Duffy, and B. Govindasamy (2002), Climate responses to a doubling of atmospheric carbon dioxide for a climatically vulnerable region, *Geophys. Res. Lett.*, *29*(11), 1514, doi:10.1029/2001GL014431.

Uppala, S., et al. (2005), The ERA-40 Re-analysis, *Q. J. R. Meteorol. Soc.*, *131*, 2961–3012, doi:10.1256/qj.04.176.

Wang, C., Y. Y. Wang, and P. F. Wang (2006), Water quality modeling and pollution control for the eastern route of South to North Water Transfer Project in China, *J. Hydrodyn.*, *18*(3), 253–261, doi:10.1016/S1001-6058(06)60001-2.

Wang, L. S., and C. Ma (1999), A study on the environmental geology of the Middle Route Project of the South-North water transfer, *Eng. Geol.*, *51*(3), 153–165, doi:10.1016/S0013-7952(98)00043-X.

Wetherald, R. T., and S. Manabe (1981), Influence of seasonal variation upon the sensitivity of a model climate, *J. Geophys. Res.*, *86*, 1194–1204, doi:10.1029/JC086iC02p01194.

Xie, Z. H., F. Yuan, Q. Y. Duan, J. Zheng, M. L. Liang, and F. Chen (2007), Regional parameter estimation of the VIC land surface model: Methodology and application to river basins in China, *J. Hydrometeorol.*, *8*(3), 447–468, doi:10.1175/JHM568.1.

Yang, L. X., and G. W. Liu (2003), *Water Transfer Project in Foreign Countries* (in Chinese), pp. 30–36, China Water Power Press, Beijing.

Yao, B. Y., and Q. L. Chen (1982), South-to-north water transfer project plans, in *Long Distance Water Transfer*, edited by A. Biswas et al., pp. 83–96, Tycooly Int., Dublin.

Yeh, T. C., R. Wetherald, and S. Manabe (1984), The effect of soil moisture on the short-term climate and hydrology change: A numerical experiment, *Mon. Weather Rev.*, *112*, 474–490, doi:10.1175/1520-0493(1984)112<0474:TEOSMO>2.0.CO;2.

Yuan, X., Z. H. Xie, J. Zheng, X. J. Tian, and Z. L. Yang (2008), Effects of water table dynamics on regional climate: A case study over East Asian monsoon area, *J. Geophys. Res.*, *113*, D21112, doi:10.1029/2008JD010180.

Zeng, X., M. Zhao, and R. Dickinson (1998), Intercomparison of bulk aerodynamic algorithms for the computation of sea surface fluxes using TOGA COARE and TAO data, *J. Clim.*, *11*, 2628–2644, doi:10.1175/1520-0442(1998)011<2628:IOBAAF>2.0.CO;2.

Zhang, D. F., X. J. Gao, Z. C. Zhao, J. S. Pal, and F. Giorgi (2005), Simulation of climate in China by RegCM3 model (in Chinese), *Adv. Clim. Change Res.*, *1*(3), 119–121.

Zhang, D. F., L. C. OuYang, X. J. Gao, Z. C. Zhao, J. S. Pal, and F. Giorgi (2007), Simulation of the atmospheric circulation over east Asia and climate in China by RegCM3 (in Chinese), *J. Trop. Meteorol.*, *23*(5), 348–356.

Zhang, H. T., C. H. Zhu, and Q. Zhang (2004), Numerical modeling of microclimate effects produced by the formation of the Three Gorges Reservoir, *Resour. Environ. Yangtze Basin*, *13*(2), 137–137.

Zhao, M. (2002), A theoretical analysis on the effect of water transportation from south to north China on the local climate in the northern part of China, *J. Nanjing Univ.*, *38*(3), 271–280.

Zheng, J., Z. H. Xie, Y. J. Dai, X. Yuan, and X. Q. Bi (2009), Coupling of the common land model (CoLM) to the regional climate model (RegCM3) and its preliminary validation (in Chinese), *Chin. J. Atmos. Sci.*, *33*(4), 737–750.

Zhou, T. J., and Z. X. Li (2002), Simulation of the east Asian summer monsoon using a variable resolution atmospheric GCM, *Clim. Dyn.*, *19*, 167–180, doi:10.1007/s00382-001-0214-8.

F. Chen and Z. Xie, ICCES, International Center for Climate and Environmental Sciences, Institute of Atmospheric Physics, Chinese Academy of Sciences, Beijing 100029, China. (zxie@lasg.iap.ac.cn)